Visual Abstract

Multi-level uncertain fatigue analysis of a truss under incomplete available information

R. B. P. Nonato
Mechanical Engineering Department, Federal Institute of Santa Catarina, IFSC, Xanxerê, Brazil
raphaelbasilio@gmail.com, https://orcid.org/0000-0002-4740-9888

ABSTRACT. The present paper deals with the prediction of the fatigue life of a planar tubular truss, when geometrical parameters, material properties, and live loads are non-deterministic. A multi-level calculation uncertainty quantification framework code was designed to aggregate the finite element method and fatigue-induced sequential failures. Due to the incompleteness of the aleatory-type inputs, the maximum entropy principle was applied. Two sensitivity analyses were performed to report the most influencing factors. In terms of variance, the results suggest that the slope of the curve crack growth rate × stress intensity factor range is the most influencing factor related to fatigue life. Furthermore, due to the application of the entropy concept, the fatigue crack growth boundaries and fatigue crack semi-width boundaries obtained provide the most unbiased fatigue crack design mapping. These boundaries allow the designer to select the worst-case fatigue scenario, besides being able to predict the crack behavior at a required confidence level.

KEYWORDS. Fatigue analysis, Uncertainty quantification, Truss, Uncertain fatigue analysis, Incomplete information, Maximum entropy principle.

Citation: Nonato, R.B.P., Multi-level Uncertain Fatigue Analysis of a Truss under Incomplete Available Information, Frattura ed Integrità Strutturale, 65 (2023) 17-37.

Received: 22.04.2023
Accepted: 06.07.2023
Online first: 19.07.2023
Published: 01.10.2023

INTRODUCTION

The fatigue phenomenon is responsible for the majority of structural systems failures due to mechanical causes [1]. Cyclic loading acting on a structure during its life may produce local failures sufficient to provoke its total collapse. One manner to mitigate this risk is to provide a certain level of redundancy, which could prevent disasters, catastrophic events, and losses in general. However, in a fatigue scenario under the fracture mechanics approach, even a structure with a high redundancy degree needs to be carefully checked with regard to its safety under uncertainty. Furthermore, under the assumption of uncertainty in involved parameters, the analysis demands more sophisticated tools and methodologies to compose the fatigue framework due to the complexity and amount of data. A complicating factor in this type of analysis occurs when the necessary information about the uncertain input quantities (UIQs) is incomplete or simply unavailable. Another factor that brings difficulty refers to the calculation framework, which intrinsically involves multiple levels through which the uncertainty has to be propagated. In this sense, uncertain fatigue analyses have been conducted to reflect this lack of information and how they impact the system response quantities (SRQs) involved in all

calculation levels. These types of analyses are mainly performed in problems related to reliability analysis, as can be checked in [2-6].
In the context of a Monte Carlo simulation or a variation of it, the uncertainty quantification (UQ) approaches applied can be listed as: (a) classical probabilistic; (b) Bayesian inference; and (c) probability bounds analysis (PBA). As far as this research could reach, most studies are based on the probabilistic methods [2, 4, 5, 7, 8]. This approach, on which this paper is based to model the uncertainties, represents an adequate UIQ when there is enough random data to characterize it. Inherently, the degree of data dispersion cannot be simply removed, although it can be reduced by, for example, improving the control of the involved process. Related to the Bayesian inference applied to fatigue reliability analysis, more accurate inferences on SRQs may be achieved by the available knowledge as the prior trustworthiness on model parameters [9-11]. Finally, PBA, which aggregates probabilistic and interval variables, is applied, for example, in [12-14].
Classical probabilistic approach is related to Monte Carlo sampling or one of its variations. It comprises a mathematical definition of aleatory uncertainties as probability distributions. Moreover, uncertainty quantification frameworks (UQFWs) comprising aleatory-type uncertainty often address the challenge of determining the probability distribution and the UIQs of this type, and it becomes more prone to errors when the input data is not available or given in an incomplete manner.
Related to aleatory-type, two distinct situations may occur: the probabilistic distribution from which an UIQ is originated is known and its parameters are unknown; the other is described by the knowledge of the distribution parameters of the UIQ, but the distribution type itself is unknown (situation analyzed here).
One of the methodologies to determine the probability density function (PDF) or cumulative density function (CDF) of the aleatory-type UIQs in a situation of incomplete or unavailable information involves the application of the maximum entropy principle (MEP), which scope involves the selection of the PDF or CDF that turns the Shannon information entropy a maximum concomitantly with the fulfillment of previously known moments of the distribution. The concepts of the MEP were firstly presented by [15], and [16]. Additional contributions posteriorly emphasized the application of the principle, e.g. [17, 18]. The focus on engineering problems was also established due to the need to represent the behavior of the related variable data. This can be evidenced in the works [19, 20]. This methodology may be useful for purposes of fatigue analysis, since the statistical information of the involved parameters is not often available either.
For life prediction and fatigue damage estimation, two main approaches are available. The S-N curve approach addresses variable load with constant amplitude, producing a constant amplitude stress range, which is related to the number of cycles to failure (fatigue life). The capability of this approach can be expanded to variable-amplitude loadings too by the application of Palmgren-Miner linear cumulative damage rule, for example. The second approach is based on fracture mechanics principles (adopted in this paper), in which a mathematical modeling of the stress field in the region of the crack tip is made.
Therefore, this paper deals with an unbiased multi-level uncertainty quantification related to fatigue limit state of a planar truss using fracture mechanics approach. The UIQs are modeled as aleatory-type and other parameters involved are deterministic, obtaining the fatigue life (SRQ). In accordance with the available information about the aleatory-type UIQs, the application of the MEP brings out the most unbiased information about the SRQs.
Two models are conceived herein. In the first, the UIQs are the live loads, initial crack semi-width (major axis half-opening), current life, fracture toughness of the material employed, pipe outside diameter, pipe thickness, the intercept and the slope of the curve crack growth rate × stress intensity factor range. Four of the eight factors mentioned are then eliminated by the application of the elementary effects method (EEM). In the second model, the first-order sensitivity indices are ranked in descending order for the four most influencing UIQs considered (the slope of the curve crack growth rate × stress intensity factor range, pipe outside diameter, pipe thickness, and initial crack semi-width).

Multi-level deterministic fatigue analysis: fracture mechanics approach with variable amplitude loading

This section describes the deterministic crack-growth model approach under variable amplitude loading applied to the structural pipe case. Furthermore, the possible limit states are addressed with the selection of two for simultaneous implementation in this work.

Deterministic Fracture Mechanics Approach

If a crack occurs under conditions in which the elastic regime is predominant, which is the majority of fatigue situations [21], the linear elastic fracture mechanics (LEFM) can be applied to mathematically model this phenomenon. This assumption implies a small plastic zone around the crack tip compared to the crack semi-width.

In this model, structural dimensions, crack semi-width, and stress characterize the overall behavior of a cracked body. The effects of these parameters define the stress intensity factor, K, applied to the case of a structural pipe, given by Eqn. 1,

$$K = Y\left(a,t,D\right)S\sqrt{\pi a} \tag{1}$$

where a is the current crack semi-width (see Fig. 1), S is the stress acting on the body, and $Y\left(a,t,D\right)$ is the geometrical function depending on the dimensions of the body (a, pipe thickness (t), and pipe outside diameter (D)), which from now on will be represented by Y, for simplification purposes. Fig. 1 shows the pipe cross-section corresponding to the cutting plane with the largest crack dimensions, in which D, t, crack width ($2a$), crack depth (b), and point (P) are represented.

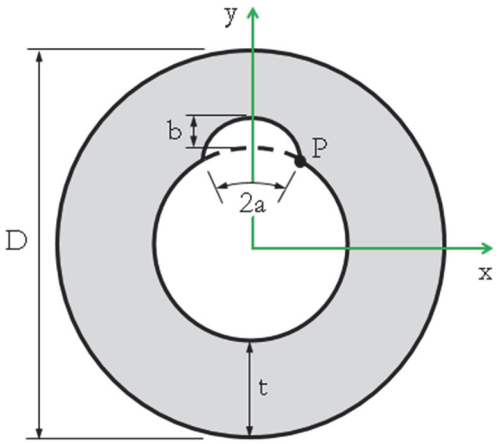

Figure 1: Dimensions of a circumferential internal surface crack at the pipe cross-section with the largest crack dimensions.

In other words, the elastic-stress field magnitude can be represented by the parameter K (K_I, K_{II}, and K_{III}, which correspond to fracture modes I, II, and III, respectively). When K reaches a threshold value known as fracture toughness (which depends on constraint level, loading rate, and service temperature), theoretically the failure occurs. For example, if the situation involves the mode I, K_I has to be compared with K_{I_C} (mode I fracture toughness).

Thenceforth, the governing crack-growth model of the crack propagation rate, also known as Paris-Erdogan law, can be described by Eqn. 2,

$$\frac{da}{dN} = C\left(K_r\right)^m \tag{2}$$

in which C is the intercept constant and m is the slope of the curve $\left(da/dN\right)\times K_r$ on a log-log scale, which are experimentally obtained as a function of frequency, environment, stress ratio, temperature, and material [22], and N is the fatigue life (number of stress cycles). Eqn. 2 is a function of stress intensity factor range, K_r, which is simply given by $K_r = K_{max} - K_{min}$, where K_{max} and K_{min} are the maximum and minimum stress intensity factors, respectively. Eqn. 1 can be transformed into Eqn. 3 to express the relation between the ranges of both stress intensity factor and applied stress:

$$K_r = Y\,S_r\sqrt{\pi a} \tag{3}$$

in which S_r is the far field stress range with both variable amplitude and frequency. As the crack does not propagate below a threshold value of stress intensity factor range (K_{rth}), Eqn. 2 can now be rewritten in terms of Eqn. 4 to discern between the stress cycles that effectively contribute to crack propagation and those that does not, i.e.

$$\frac{da}{dN} = \begin{cases} 0, \; if \; K_r < K_{rth} \\ C\left(K_r\right)^m, \; otherwise \end{cases} \tag{4}$$

In other words, to account only for the effective stress cycles, we will adopt the strategy applied in [23], which discards the non-contributors' stress cycles from the analysis. Therefore, the threshold of the stress range, S_{rth}, is given by Eqn. 5:

$$S_{rth} = \frac{K_{rth}}{Y\sqrt{\pi a}} \tag{5}$$

Effective Stress Cycles and Fatigue Limit State

The concept of effective stress range takes into account only the stress ranges equal to or greater than the threshold value, corresponding to those which effectively contribute to the crack growth process. Eqn. 6 redefines the stress range, S_r, in terms of the effective stress range, S_{re}:

$$S_r := S_{re} = \frac{\int_{S_{rth}}^{S_{rmax}} \left(S_r\right)^m f_{S_r}\left(s_r\right) ds_r}{\int_{S_{rth}}^{S_{rmax}} f_{S_r}\left(s_r\right) ds_r} \tag{6}$$

where f_{S_r} is the stress range probability distribution, and S_{rmax} is the maximum value of the stress range, such that the fatigue life N (Eqn. 7) can be redefined in terms of the effective fatigue life N_e and expressed by implementing this concept to the non-null part of Eqn. 4, yielding Eqn. 7:

$$N := N_e = \int_{a_0}^{a_f} \frac{da}{C\left(K_r\right)^m} = \int_{a_0}^{a_f} \frac{da}{C\left(Y S_r \sqrt{\pi a}\right)^m} \tag{7}$$

where a_0 is the initial crack semi-width, a_f is the final crack semi-width, and N is updated to be the expected fatigue life due to only effective stress cycles.

Within the scope of LEFM, fatigue limit state can be stated in terms of a comparison between: (a) current crack semi-width and final (critical) crack semi-width; (b) current stress intensity factor at the leading edge of the crack and fracture toughness of the material; (c) current number of effective stress cycles and required fatigue life. In this paper, the fatigue limit state function Q is formulated based on the first two options (because the current number of effective stress cycles are supposed to be unknown), prevailing the most restrictive criterion. This corresponds to Eqn. 8, in which a is the current crack semi-width, α is the set of admissible current crack semi-widths, and κ is the set of admissible mode I stress intensity factors.

$$Q = \inf_{a \in \alpha; K_I \in \kappa} \left[N\left(a_f - a\right), N\left(K_{I_C} - K_I\right) \right]. \tag{8}$$

MULTI-LEVEL UNCERTAIN FATIGUE ANALYSIS: FRACTURE MECHANICS APPROACH AND SENSITIVITY ANALYSIS

This section presents UQ, UIQ, and SRQ definitions, some of the existing methods of uncertainty propagation, besides establishing the general relationship between the UIQs and SRQ in the context of a non-deterministic fatigue analysis via fracture mechanics. Complementarily, the multi-level formulation is associated with the uncertain fatigue problem.

UQ, UIQs, and SRQs

In the field of model-based predictions, uncertainty originates from model inputs (boundary conditions, initial conditions, etc.), gap between real system and adopted model, computational costs (time to accomplish the run, analysis feasibility,

and complexity), solution, and errors [24]. It is important to assess the impact of these sources of uncertainty in the context of prediction and safety issues [25]. Uncertainties can also be generated under the consideration of experimental/design multiplicative factors, which values are generally attributed by experienced personnel representing committees, institutions, or normative councils, for example.

Among a wide scope of uncertainty propagation methods, we can mention Monte Carlo sampling (MCS), Latin hyper-cube sampling (LHS), quasi Monte Carlo sampling (QMCS), analytical uncertainty propagation (AUP), fuzzy interval arithmetic (FIA), polynomial chaos (PC), and subset simulation (SS), for example, applied in [26-29].

Within the scope of this paper, the aleatory-type uncertainty is generally described by a PDF and/or CDF. The related model has inherent variability, such that it is intrinsic to the nature of the problem. Independently of the reliability of the information, the aleatory-type uncertainty cannot be directly eliminated, although it may be better quantified in order to be reduced. This type of uncertainty is modeled based on the information originated at a candidate, selected, or available probability distribution. From this perspective, let n_{a_i} be the number of available parameters of the i-th probabilistic UIQ X_i (random variable). Denoting the PDF of this UIQ by f_{X_i}, the outcomes x_i of X_i are extracted from Eqn. 9:

$$x_i = f_{X_i}^{-1}\left(x_i, a_i, \cdots, n_{a_i}\right) \tag{9}$$

where a_i is the a-th available parameter related to the random variable X_i, and n_{a_i} refers to the number of available parameters associated to X_i. Therefore, x_i represents the possible realizations of a universal set χ_i of all possible outcomes. In this sense, a CDF F_{X_i} can be assigned to every element x_i, as long as the following conditions are concomitantly satisfied: $F_{X_i}\left(x_i, a_i, \cdots, n_{a_i}\right) \in [0,1], \forall x_i \in \chi_i$, and $\sum_{x_i \in \chi_i} F_{X_i}\left(x_i, a_i, \cdots, n_{a_i}\right) = 1$.

In its truncated form, the additional condition $\chi_i = \left\{x_i \in \middle| \, x_i^{LB} \le x_i \le x_i^{UB}\right\}$ must be fulfilled, which is described by the fact that all possible outcomes must be inside the established acceptance interval. The limits x_i^{LB} and x_i^{UB} are the lower and upper bounds of the possible outcomes, respectively, where $\mathbb{R}$ is the set of all closed real numbers.

Multi-level uncertain fracture mechanics approach

The inputs to a fracture mechanics analysis are frequently subjected to considerable uncertainty. Thenceforth, conservative estimation of these quantities are often employed, sometimes resulting in improbable outputs related to fatigue [30]. One of the possible manners to obtain a more realistic result is structured under the assumption of uncertain inputs propagated throughout an UQFW.

In uncertainty quantification (UQ), predictions are generally based on models, which are used to obtain the corresponding required uncertainties [31]. The characterization of uncertainties within a UQ process may address different types of UIQs throughout distinct calculation levels. In this paper, the strategy introduced by [14] is extended to multiple levels of calculation, and it is now implemented to fracture mechanics in the context of fatigue-induced sequential failures of the structural elements involved. Each round of calculation corresponds to the failure of one or more structural elements simultaneously. Although this last situation is mathematically possible, the probability of simultaneously multiple element failure occurring tends to zero because of the distinct sources of uncertainty considered in each model. Moreover, inside each round there are multiple levels of calculation to lead this structural component to failure.

The mapping of the UIQs all over the uncertainty propagation process results in the values of the SRQs of all involved levels. Therefore, in the first round, the SRQs obtained at the first level feed the second level as UIQs, i.e. the SRQs calculated at the second level are not only affected by the UIQs of the same level, but also by the SRQs of the previous level. The process goes on analogously for the next levels. The subsequent rounds refer to the next failures of the structural elements until the structural redundancy level becomes negative (a mechanism is then formed and, consequently, the structure loses its functionality). Each round has its own levels in order to reach the corresponding member failure; however, some SRQs from previous rounds related to structural members that have not yet failed are also input for subsequent rounds. This is schematically described in Fig. 2.

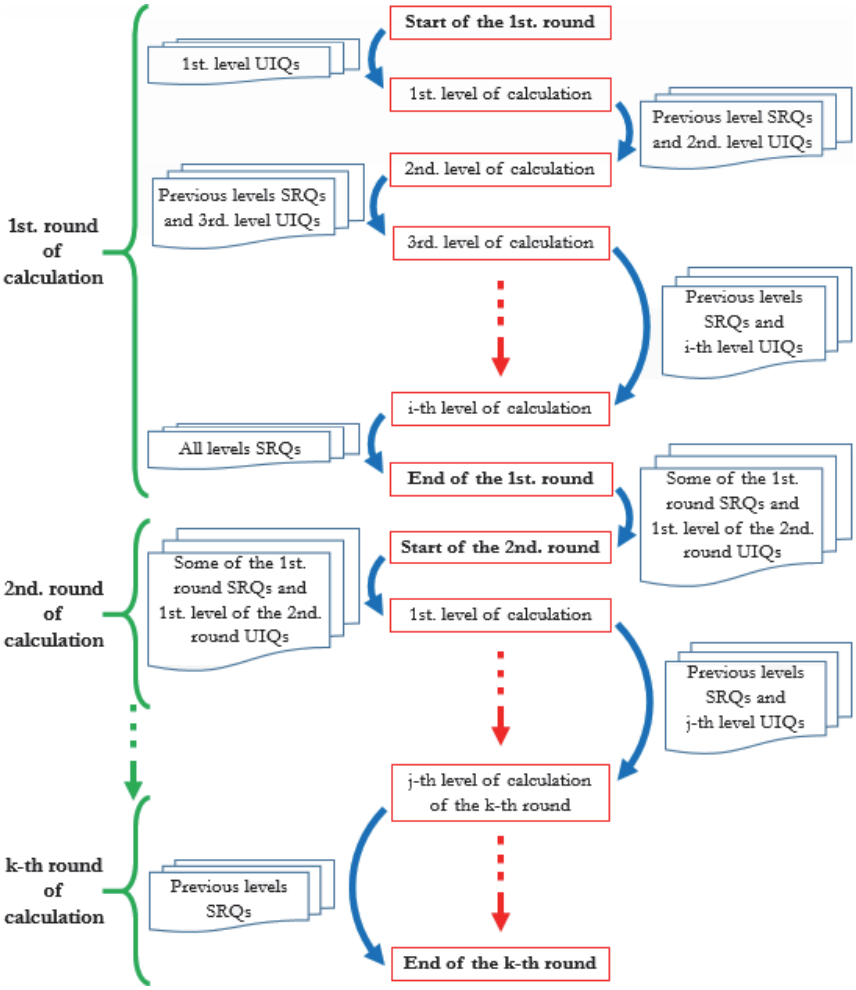

Figure 2: Flowchart of multi-level uncertain calculation for one round and its interface with the subsequent rounds.

In the present paper, the propagation is made via Latin Hypercube Sampling (LHS), which is partially justified by its easy implementation and the achievement of the convergence of results without a large computational effort, requiring reasonable sample sizes. Therefore, the mapping of the n_i aleatory-type UIQs of the level being calculated and the n_j SRQs from the previous level(s) of calculation that are UIQs in the current level of calculation (from the second level onwards) into the n_k SRQs of the current level of calculation is expressed by the following mathematical model (Eqn. 10):

$$\mathbb{M} = \left(\boldsymbol{X}_1, \boldsymbol{X}_2, \cdots, \boldsymbol{X}_i, \cdots, \boldsymbol{X}_{n_i}, \boldsymbol{Y}_1, \boldsymbol{Y}_2, \cdots, \boldsymbol{Y}_j, \cdots, \boldsymbol{Y}_{n_j} \right) \rightarrow \boldsymbol{Z}_1, \boldsymbol{Z}_2, \cdots \boldsymbol{Z}_k, \cdots, \boldsymbol{Z}_{n_k} \tag{10}$$

where $\boldsymbol{X}_i$ is the column vector of the i-th aleatory-type UIQ, $\boldsymbol{Y}_j$ is the column vector of the j-th aleatory-type UIQ in this level that had already been an SRQ at a previous level, $\mathbb{M}$ is the mathematical model which depends on the nature of the problem, and $\boldsymbol{Z}_k$ is the column vector of the k-th SRQ. Each UIQ or SRQ is a column vector of the form (Eqn. 11):

$$\boldsymbol{V}_q = \left[v_q^{(1)}, v_q^{(2)}, \cdots, v_q^{(r)}, \cdots, v_q^{(n_r-1)}, v_q^{(n_r)} \right]^T \tag{11}$$

in which the superscript between parentheses means the realization number, r is the r-th realization, and n_r is the number of realizations, such that the condition $r \in \mid 1 \leq \mathrm{r} \leq n_r$ holds, where $\mathbb{N}$ is the closed set of natural numbers. In other words, the column vector $\boldsymbol{V}_q$ can represent $\boldsymbol{X}_i$, $\boldsymbol{Y}_j$, or $\boldsymbol{Z}_k$. Analogously, for example, $v_q^{(r)}$ can assume $x_i^{(r)}$, $y_j^{(r)}$, or $z_k^{(r)}$. If the

uncertainty propagation produces n_{ik} SRQs throughout all levels and rounds, then $n_{ik} \times n_r$ values are obtained as response. If a parameter presents a variation which magnitude can be neglected for the purposes of the analysis being conducted or its value is known exactly, then it can be assumed as a deterministic quantity. Generally, computational capacity and objectives of the analysis guide through the decision of considering a parameter as deterministic.
The application of the mathematical model of Eqn. 10 in the first level is related to the calculation of the UIQ stress range $\boldsymbol{S}_r$, which can be expressed in terms of geometrical parameters and applied loads, as shown in Eqn. 12,

$$\boldsymbol{S}_r = \left[\boldsymbol{G}_1, \boldsymbol{G}_2, \cdots, \boldsymbol{G}_s, \cdots, \boldsymbol{G}_{n_s}, \boldsymbol{P}_1, \boldsymbol{P}_2, \boldsymbol{P}_t, \cdots, \boldsymbol{P}_{n_t}\right], \boldsymbol{S}_{rth}^{(r)} < \left|\boldsymbol{S}_r^{(r)}\right| \left\langle \boldsymbol{S}_{ru}^{(r)}, \forall r \in \left| 1 \le \mathrm{r} \le n_r \right.\right. \tag{12}$$

where $\boldsymbol{S}_{rth}$ (presented in Eqn. 5) and $\boldsymbol{S}_{ru}$ are ranges that, respectively, refer to the threshold (below which the crack does not grow) and ultimate stress (which causes material rupture), n_s is the number of geometrical parameters, n_t is the number of applied loads, $\boldsymbol{G}_s$ is the vector of the s-th geometrical parameter, and $\boldsymbol{P}_t$ is the vector of the t-th applied load. When Eqn. 10 is applied to the subsequent levels, $\boldsymbol{S}_r$ is now an UIQ of the SRQ $\boldsymbol{K}_r$ (see Eqn. 13). The other UIQs are $\boldsymbol{a}$, and $\boldsymbol{Y}$. In other words, as $\boldsymbol{Y}$ and $\boldsymbol{S}_r$ are SRQs in the first level of each round, $\boldsymbol{K}_r$ is an SRQ in the second level of the referred round. Therefore, $\boldsymbol{K}_r$ is a function of $\boldsymbol{Y}$, $\boldsymbol{S}_r$, and $\boldsymbol{a}$ (Eqn. 13):

$$\boldsymbol{K}_r = f\left(\boldsymbol{Y}, \boldsymbol{S}_r, \boldsymbol{a}\right) \tag{13}$$

In the case of Eqn. 2 (already updated for the concept of number of effective cycles, $\boldsymbol{N}$), the SRQ $\boldsymbol{da}/\boldsymbol{dN}$ requires three UIQs: $\boldsymbol{K}_r$ (3rd. level), $\boldsymbol{C}$ (1st. level), and $\boldsymbol{m}$ (1st. level). Therefore, $\boldsymbol{da}/\boldsymbol{dN}$ is an SRQ in the third level because it depends on at least one SRQ from the second level ($\boldsymbol{K}_r$ in Eqn. 14), and the fourth level of calculation refers to the obtainment of the SRQ number of cycles $\boldsymbol{N}$ from the term $\boldsymbol{da}/\boldsymbol{dN}$ (Eqn. 15), which finishes one round of calculation. The current values of crack semi-widths, stress intensity factor and current number of effective stress cycles are updated for the structural members that have not failed yet. Thenceforth, the process restarts to a new round of calculation.

$$\frac{\boldsymbol{da}}{\boldsymbol{dN}} = f\left(\boldsymbol{K}_r, \boldsymbol{C}, \boldsymbol{m}\right) \tag{14}$$

$$\boldsymbol{N} = f\left(\frac{\boldsymbol{da}}{\boldsymbol{dN}}\right) \tag{15}$$

Sensitivity analysis

In the context of an uncertain fatigue analysis, the sensitivity analysis (SA) is determinant to both feasibility and time of analysis, in order to focus on the most influencing UIQs [32, 33]. Parameters involved in fatigue analyses of structural systems were subjected to SAs in order to verify how the uncertainty in the considered UIQs influence the calculated SRQs. Fatigue life of complex mechanical components were subjected to a reliability-based sensitivity [34]. Material and geometrical UIQs were considered the most influencing factors in the life of hollow extrusion dies [35]. A reliability-based fatigue assessment methodology of steel bridges was also proposed [36]. API steels in gaseous hydrogen were also objects of a SA related to its fatigue crack growth model [37]. A study of the variability of the microstructural components relatively to fatigue phenomenon through a SA was performed [38]. A SA of fatigue crack initiation was conducted related to notch morphology parameters of a double-notched specimen [39]. A fatigue reliability analysis followed by a SA was accomplished on models of turbine discs considering multi-source uncertainties [40].
In this paper, a double SA was accomplished: the first computational model was subjected to the elementary effects method (EEM) aiming at eliminating four of the eight UIQs to decrease the computational cost. Thenceforth, the four most relevant UIQs were considered in a second model, in which the first-order sensitivity indices were calculated to obtain the relative importance of each uncertain parameter for this design.
The EEM was introduced by Morris [41], aiming at discerning which UIQs have effects: (a) negligible; (b) linear; or (c) nonlinear. The ik-th elementary effect of the i-th UIQ related to the k-th SRQ is given by Eqn. 16:

$$EE_{ik} = \frac{\boldsymbol{Z}_k\left(\boldsymbol{X}_1,\cdots,\boldsymbol{X}_{i-1},\ \boldsymbol{X}_i+\Delta,\cdots,\boldsymbol{X}_{n_i}\right)-\boldsymbol{Z}_k\left(\boldsymbol{X}_1,\cdots,\boldsymbol{X}_{i-1},\ \boldsymbol{X}_i,\cdots,\boldsymbol{X}_{n_i}\right)}{\Delta} \tag{16}$$

in which Δ is a vector of values within the interval associated with the UIQ $\boldsymbol{X}_i$, and $\boldsymbol{Z}_k$ is the SRQ.

One of the variance-based methods, the first-order sensitivity index, can be defined by the variance of the conditional expectation of each UIQ related to the variance of the common SRQ. Mathematically, Eqn. 17 provides the ik-th first-order index corresponding to the effect of the UIQ $\boldsymbol{X}_i$ related to the SRQ $\boldsymbol{Z}_k$, where $V[.]$ and $E[.]$ mean, respectively, the variance and the expected value operators. This can be understood as the variance of the expectation of the k-th SRQ conditioned to the occurrence of the i-th UIQ related to the entire variance of the SRQ.

$$S_{ik} = \frac{V\left[E\left(\boldsymbol{Z}_k \mid \boldsymbol{X}_i\right)\right]}{V\left(\boldsymbol{Z}_k\right)} \tag{17}$$

MAXIMUM ENTROPY PRINCIPLE

This section associates the maximum entropy principle (MEP) with UQ. The general framework of MEP applied to known support and moments of a distribution is presented in order to evidence the particular case where only interval and mean of data are concomitantly known, a situation applied in this paper to represent the UIQs.

MEP in the context of uncertainty

In the case where insufficient number of probabilistic distribution moments are the only information available, the MEP can shape the most unbiased distribution, meeting this given data [42]. The contributions strictly related to structural systems has an ever-growing potential, which has been highlighted by the greater attention deserved through last years. Based on the MEP, a belief reliability distribution was proposed to measure system performance from the influences of design margin, aleatory and epistemic uncertainties [43]. PDFs were estimated using more than four moments of distribution and a reliability-based design optimization was performed using the MEP and compared to that originated by the finite difference method [44]. The MEP was also applied to obtain the reliability bound with respect to the first moment truncated for the first time. The reliability of machine components via MEP was studied too [45], in which a PDF and a failure probability model were established. A structural reliability analysis was performed based on the MEP using polynomial chaos expansion, e.g. [46]. In addition, the MEP and the Dempster-Shafer theory were combined to perform a reliability analysis [47].

General framework of MEP applied to known support and moments of a distribution

In the case where a continuous PDF of a variable is unknown and a set of its parameters is available (support and/or moments distributions), it is possible to apply the MEP in order to find the distribution using the restrictions provided by this information, according to the processes proposed in [16, 48].

Let X_i be a random variable, which has $f_{X_i}\left(x_i\right)$ as its PDF and $F_{X_i}\left(x_i\right)$ as its CDF. The entropy H is the quantity of uncertainty inherent to a process result. Let X_i be delimited by a support interval $\left[X_i^{LB}, X_i^{UB}\right]$, which can be the only available information or one item of a set of information about the distribution. Therefore, the entropy is quantified in Eqn. 18:

$$H = -\int_{X_i^{LB}}^{X_i^{UB}} f_{X_i}\left(x_i\right) log\left(f_{X_i}\left(x_i\right)\right) dx_i = -\int_{X_i^{LB}}^{X_i^{UB}} log\left(f_{X_i}\left(x_i\right)\right) dF_{X_i}\,. \tag{18}$$

For example, H can be interpreted as the average information provided by the realization of an experiment or simulation. It is the average uncertainty removed or average amount of information aggregated by observing the outcomes of X_i. In addition, if information about the moments of the PDF is also available, $\tilde{X}_{im}$, then it is given by Eqn. 19. The m-th moment

of the i-th variable assumes the null value when $g_m(x_i)=1$, and $\tilde{X}_{i0}=1$, where the functions $g_m(x_i)$ represent the available distribution moments, being n_m the quantity of known moments.

$$\int_{X_i^{LB}}^{X_i^{UB}} g_m(x_i) f_{X_i}(x_i) dx_i = \tilde{X}_{im}, \qquad m=0,1,\cdots,n_m \tag{19}$$

In information theory, the MEP is applied to discover the PDF $f_{X_i}(x_i)$ that leads the information entropy to its maximum, observing the set of restrictions presented in Eqn. 19. This problem can be solved using the variational calculus, building the functional $\Phi\left[f_{X_i}(x_i)\right]$, which encompasses the referred restrictions using the Lagrange multiplier method by the following manner (Eqn. 20):

$$\Phi\left[f_{X_i}(x_i)\right] = -\int_{X_i^{LB}}^{X_i^{UB}} f_{X_i}(x_i) log\left(f_{X_i}(x_i)\right) dx_i + \sum_{m=0}^{n_m} \lambda_{im} \left[\int_{X_i^{LB}}^{X_i^{UB}} g_m(x_i) f_{X_i}(x_i) dx_i - \tilde{X}_{im}\right] \tag{20}$$

The aim is to find the PDF $f_{X_i}(x_i)$ that does not violate the restrictions and maximize the information entropy. This implies finding the m Lagrange multipliers λ_{im} of the i-th variable, X_i, and the values of the PDF $f_{X_i}(x_i)$ to achieve the extreme of the functional $\Phi\left[f_{X_i}(x_i)\right]$, observing the set of restrictions. This is accomplished by assuming an arbitrary perturbation $\beta\delta f_{X_i}(x_i)$ to which the null value is attributed at the extrema of the support interval. Thus, the first variation $\delta f_{X_i}(x_i)$ of this functional is given by Eqn. 21. In terms of Lagrange multipliers, this calculation yields Eqn. 22.

$$\delta\Phi\left[f_{X_i}(x_i)\right] = \left\{\frac{\partial\Phi\left[f_{X_i}(x_i)+\beta\delta f_{X_i}(x_i)\right]}{\partial\beta}\right\}_{\beta=0} = 0 \tag{21}$$

$$\delta\Phi\left[f_{X_i}(x_i)\right] = \delta f_{X_i}(x_i)\left\{-log\left[f_{X_i}(x_i)\right] - 1 + \sum_{m=0}^{n_m} \lambda_{im}\, g_m(x_i)\right\} dx_i = 0 \tag{22}$$

The term inside the brackets must vanish because of the arbitrariness of the perturbation $\delta f_{X_i}(x_i)$. Therefore, the PDF is expressed by Eqn. 23, where the n_m constants λ_{im} of the i-th variable are calculated from the available information about the moments of the distribution. Commonly, the Lagrange multipliers are obtained from the solution of a nonlinear system of algebraic equations. The next subsection is dedicated to the solution of the case applied here: known interval and mean.

$$f_{X_i}(x_i) = exp\left[-1 + \sum_{m=0}^{n_m} \lambda_{im} g_m(x_i)\right] \tag{23}$$

Maximum Entropy Distribution (Known Interval and Mean)

If a positive mean is specified in addition to the constrained interval, the following constraints are required, i.e. individual probabilities have to add up 1 and mean definition, respectively, Eqns. 24 and 25,

$$\sum_{r=1}^{n_r} \left(p_{X_i}\right)_r = 1 \tag{24}$$

$$\sum_{r=1}^{n_r} (x_i)_r \left(p_{X_i}\right)_r = \tilde{X}_{i1} \tag{25}$$

where $\left(p_{X_i}\right)_r$ is the r-th probability of the i-th UIQ and $\left(x_i\right)_r$ is the r-th outcome (realization) of the i-th UIQ. In order to solve this problem, the method of Lagrange multipliers is used, which in this context consists of calculating the derivative of the following function, (Eqn. 26),

$$F = H + \left[1 - ln(B)\right]\sum_{r=1}^{n_r}\left(p_{X_i}\right)_r + \lambda_{im}\sum_{r=1}^{n_r}\left(x_i\right)_r\left(p_{X_i}\right)_r \tag{26}$$

where λ_{im} is the Lagrange multiplier associated to the constrained mean. The constant B is fixed by the condition $\sum_{r=1}^{n_r}\left(p_{X_i}\right)_r = 1$ in what refers to the term $\sum_{r=1}^{n_r} exp\left[\lambda_{im}\left(x_i\right)_r\right]$. The differentiation of Eqn. 26 yields Eqn. 27:

$$\delta F = \left\{-ln\left[\left(p_{X_i}\right)_r\right] - ln(B) + \lambda_{im}\left(x_i\right)_r\right\}\delta\left(p_{X_i}\right)_r \tag{27}$$

Thenceforth, the maximum entropy distribution for the described constraints is expressed by Eqn. 28, which is exponential. The Lagrange multiplier λ_{im} is obtained from the mean (Eqn. 25). Therefore, if the support interval and the first moment are the only information available, the truncated exponential probabilistic distribution maximizes the uncertainty.

$$\left(p_{X_i}\right)_r = \frac{1}{B} exp\left[\lambda_{im}\left(x_i\right)_r\right]. \tag{28}$$

NUMERICAL EXAMPLE

The primary description of the tubular plane truss problem is made, presenting all the input data and establishing the calculation scope. This includes material, geometrical, and loading parameters. Moreover, the strategy to apply the multi-level UQFW to solve the problem is detailed.

Description of the Problem

Fig. 3 illustrates the bi-dimensional example to be numerically solved by the application of the multi-level probabilistic uncertainty quantification framework. The prismatic tubular structural elements are made of ASTM A36 and pinned to the rigid supports. It is a 3-element and 4-node truss system, where two concentrated loads are applied to the unique free node. Loads $\tilde{P}_{1_X}$ (horizontally directed to the left) and $\tilde{P}_{1_Y}$ (vertically pointed down), which are represented in Fig. 3, are the expected values of $\boldsymbol{P}_{1_X}$, and $\boldsymbol{P}_{1_Y}$, respectively. They are modeled as variables with constant amplitude with stress ratio $R = 0.05$, i.e. given the uncertain maximum load magnitude, the minimum load magnitude is obtained through the ratio R. Each element is characterized geometrically by its length $L^{(e)}$, outside diameter $D^{(e)}$, thickness $t^{(e)}$, initial crack semi-width $a_0^{(e)}$ at the inner surface of the element, initial crack depth $b^{(e)}$ and, in terms of material, by its fracture toughness $K_{I_C}^{(e)}$, elasticity modulus $E^{(e)}$, yield strength $S_y^{(e)}$, ultimate strength $S_u^{(e)}$, intercept constant $C^{(e)}$, and slope $m^{(e)}$.

Moreover, it is important to emphasize that the only two limit states (crack semi-width and stress intensity factor) are related to fatigue, being neglected possible serviceability requirements such as strain or displacement. For simplification of calculation, body forces are also neglected.

In Fig. 3, the number inscribed in the circle indicates the structural element; and the numbers adjacent to them represent the four nodes. As a 2-D truss problem, there are two possible displacements at each node. However, only node 1 is free to displace in both degrees of freedom. Angles θ_{32} and θ_{31} go from the bar three to two and from the bar three to one, respectively. The origin of the coordinate system is coincident with node 1. The defect is modeled by a circumferential surface crack at the internal surface of each structural pipe (see Fig. 3) far enough from their ends, in order to avoid the combination of effects from the crack and the holes used for pin joining. Although this type of discrepancy can be detected, depending on the diameter and the length of the pipe, the repair may not be feasible by conventional methods.

Tab. 1 shows the values of the deterministic parameters considered. In this table, the data can be distinguished by geometric, loading (stress ratio), and material branches. In the branch of geometric deterministic parameters, b was not considered as

a UIQ because the intention of this research was to isolate the effect of the UIQ $\boldsymbol{a}_0$. In what refers to material properties, the parameters S_y, S_u, and E were not assumed as UIQs for reasons of simplification of calculation and analysis feasibility, otherwise they would impact the overall variance and turn the analysis less feasible. The values of $\tilde{C}$, $\tilde{m}$, $\tilde{S}_y$, $\tilde{S}_u$, and R are extracted from [49]. Elasticity modulus E is collected from [50]. Finally, Mode I fracture toughness K_{I_C} was taken from [51].

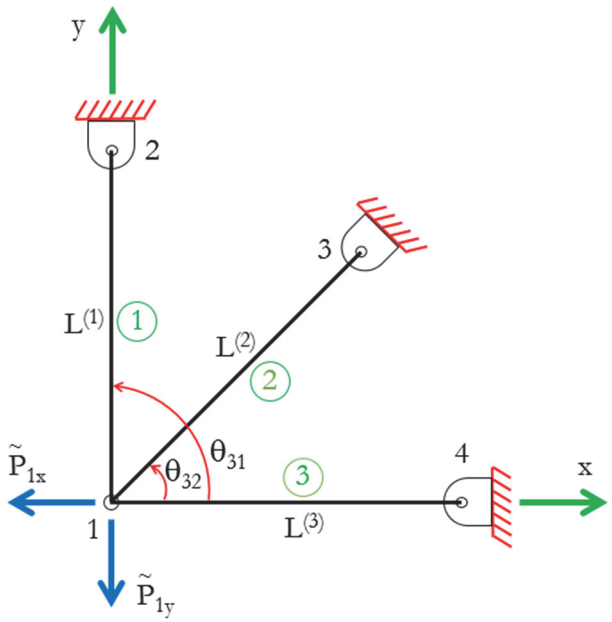

Figure 3: 2-D tubular truss system with two concentrated loads showing the nomenclature of the geometrical parameters.

Deterministic parameter	*Value*
θ_{31}	$\pi / 2$
θ_{32}	$\pi / 4$
a_f	$7.5\,mm$
b (see Fig. 1)	$2.5\,mm$
$L^{(1)} = L^{(2)} = L^{(3)}$	$3000\,mm$
R	0.05
S_y	$250\,MPa$
S_u	$400\,MPa$
E	$200\,GPa$

Table 1: Values of deterministic parameters for the planar truss example.

Tab. 2 aggregates all the available information about the UIQs, the corresponding SRQs, their relation level, range of each UIQ, and its expected value. For example, the UIQ $\boldsymbol{a}_0$, which has a range $[2.4,2.7]\,mm$ and an expected value of $\tilde{a}_0 = 2.5\,mm$, is applied to obtain the SRQs $\boldsymbol{Y}$ and $\boldsymbol{K}_r$, both at first level. It is assumed that all elements have the same crack dimensions and localization, and are constituted by the same material. Although there is a multi-level calculation framework, the focus is established on the SRQ $\boldsymbol{N}$ (4th. level) in terms of main results presented.

UIQ	*SRQ*	*Level*	*Expected value of UIQ*	*Range of UIQ*
P_{1_X}	S_r	1	$\tilde{P}_{1_X} = -200000\,N$	$\left[P_{1_X}^{LB}, P_{1_X}^{UB}\right] = [-205000, -197000]\,N$
P_{1_Y}	S_r	1	$\tilde{P}_{1_Y} = -400000\,N$	$\left[P_{1_Y}^{LB}, P_{1_Y}^{UB}\right] = [-410000, -394000]\,N$
D	S_r, Y	1, 1	$\tilde{D} = 273\,mm$	$\left[D^{LB}, D^{UB}\right] = [372.318, 274.365]\,mm$
t	S_r, Y	1, 1	$\tilde{t} = 12.5\,mm$	$\left[t^{LB}, t^{UB}\right] = [12.3, 12.9]\,mm$
a_0	Y, K_r	1, 1	$a_0 = 2.5\,mm$	$\left[a^{LB}, a^{UB}\right] = [2.4, 2.7]\,mm$
C	da/dN	1	$\tilde{C} = 1.897\times10^{-3}$	$\left[C^{LB}, C^{UB}\right] = [1.892, 1.906]\times10^{-13}$
m	da/dN	1	$\tilde{m} = 3.0000$	$\left[m^{LB}, m^{UB}\right] = [2.9925, 3.0150]$
K_{I_C}	K	1	$\tilde{K}_{I_C} = 1581.139\,MPa\sqrt{mm}$	$\left[K_{I_C}^{LB}, K_{I_C}^{UB}\right] = [1500.000, 1694.665]\,MPa\sqrt{mm}$
N_0	N	1	$\tilde{N}_0 = 500000\,cycles$	$\left[N_0^{LB}, N_0^{UB}\right] = [495000, 510000]\,cycles$
Y	K_r	2	Not applicable	Not applicable
S_r	K_r	2	Not applicable	Not applicable
K_r	da/dN	3	Not applicable	Not applicable
da/dN	N	4	Not applicable	Not applicable

Table 2: Available information about the UIQs and their relation level with the SRQs for the planar truss example.

Strategy to Apply the UQFW to the Problem Described

The overall strategy can be seen in Fig. 4. First, the sources of uncertainty are selected and the least unbiased probabilistic model is assigned to the UIQs. Using this model, UIQs values are estimated and uncertainty in the first model is propagated via LHS technique. Enough rounds of the multi-level uncertain calculation scheme are performed in this step (Fig. 2). The quantified SRQs along with the UIQs take part in the elementary effects method to eliminate the four least influencing of the eight UIQs. Thus, the remaining UIQs are considered throughout a second model also via LHS. As in the first model, this step also applies the multi-level uncertain calculation framework shown in Fig. 2. After this, the SRQs are once again quantified. A second SA is performed to obtain the first-order SA indices, which aims at finding the rank of the most influencing UIQs related to the SRQs. The design boundaries are then built and the information is recorded for further analyses. Except for the first, all the stages in this flowchart are executed via code developed within MATLAB® script.

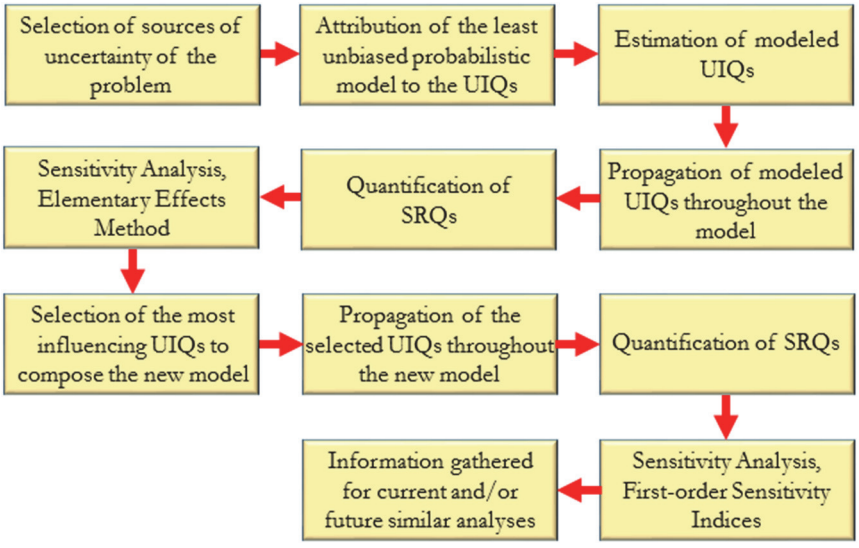

Figure 4: Flowchart representing the uncertainty quantification framework.

RESULTS AND DISCUSSION

This section presents the calculation results for the problem described, including UIQs, SRQs and the first level of SA for the first model, with eight UIQs. Subsequently, these results are shown for the second model (with just four UIQs), as well as FCGBs and FCSBs.

Results for the UIQs and SRQs in the First Model (with eight UIQs)

The involved stresses were obtained by the application of the finite element method (FEM) and the UIQs modeled were selected for this problem according to Tab. 2, as already mentioned. The MEP was applied to generate the most unbiased input data. In addition, Tab. 3 presents the frequencies of each aleatory-type UIQ in order to compose the rank from the EEM, which was accomplished for 10000 realizations. Under the criterion of the most frequent outcome, the four most influencing UIQs are, in decreasing order: (a) $\boldsymbol{m}$, which frequency is 9371 realizations in the first place of the ranking; (b) $\boldsymbol{a_0}$, presenting 6603 realizations in the second place of the ranking; (c) $\boldsymbol{t}$, with 6220 realizations.in the third place of the ranking; and (d) $\boldsymbol{D}$, corresponding to 8351 realizations in the fourth place of the ranking.

Rank	*Number of realizations*							
	$\boldsymbol{D}$	$\boldsymbol{t}$	$\boldsymbol{a_0}$	$\boldsymbol{N_0}$	$\boldsymbol{K_{I_C}}$	$\boldsymbol{P_{1_X}}, \boldsymbol{P_{1_Y}}$	$\boldsymbol{C}$	$\boldsymbol{m}$
1	55	184	389	0	1	0	0	9371
2	530	2255	6603	0	4	0	0	608
3	1022	6220	2727	0	10	0	0	21
4	8351	1338	281	0	30	0	0	0
5	42	3	0	2	147	5	9801	0
6	0	0	0	62	9617	124	197	0
7	0	0	0	2702	190	7106	2	0
8	0	0	0	7234	1	2765	0	0

Table 3: Matrix of frequencies (number of realizations) to compose the EEM rank for the planar truss example.

Based on the results from the EEM, the second model was created with the uncertainty related to these four UIQs being propagated, yet observing the information previously given by Tabs. 1 and 2. The other four (least influencing) were then assumed as deterministic quantities. Therefore, 10000 new realizations were obtained for each parameter via simulation of the second model, such that the results presented from now on are referred to this model.

Results for UIQs and SRQs in the Second Model (with four UIQs)

The EME distributions associated with histograms of UIQs $\boldsymbol{m}$, $\boldsymbol{t}$, $\boldsymbol{a_0}$, and $\boldsymbol{D}$ are illustrated in Figs. 5 and 6, where the solid blue line represents the PDF, and the yellow bars compose the histogram. The dotted vertical black line (lower bound) and the continuous vertical black line (upper bound) delimit the range covered by the truncated distribution. In addition, the vertical lines (the continuous red and the dashed green ones) correspond to the deterministic value and its mean value, respectively. These representations are referred to the sample of the structural element 2, as well as could have been taken from another structural element, since they all have variable parameters. As Kernel smoothing function was applied to all the PDFs of this paper, the lower and upper limits are surpassing the interval covered by the histogram due to tails smoothing. Confirming the condition of the mean not coincident with the median, the mode is at the left of the mean.

The behavior of the SRQ $\boldsymbol{N}$ is represented in Fig. 7, which shows the histogram with its corresponding estimated PDF. This plot observes the same convention of the line styles of the plots of the UIQs, except for the bounds (not represented because they are the output in the calculation). Although all the UIQs were modeled as EME distributions, the histogram and estimated PDF of the SRQ $\boldsymbol{N}$ do not address the same behavior.

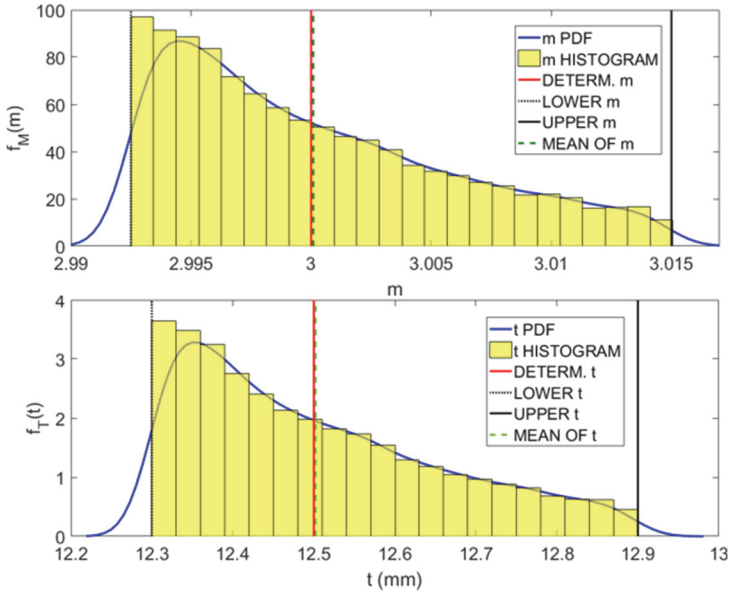

Figure 5: Histograms and PDFs of the UIQs $\boldsymbol{m}$ and $\boldsymbol{t}$ with indications: deterministic, lower bound, upper bound, mean (element 2).

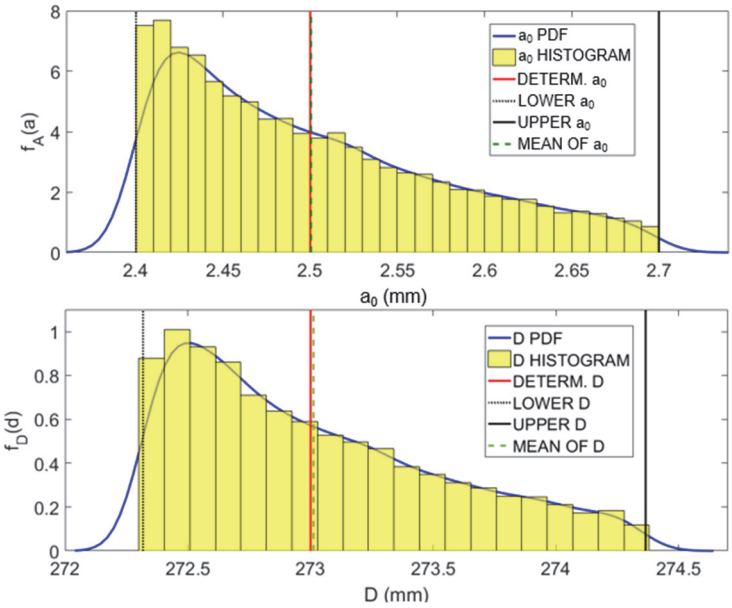

Figure 6: Histograms and PDFs of the UIQs $\boldsymbol{a_0}$ and $\boldsymbol{D}$ with indications: deterministic, lower bound, upper bound, mean (element 2).

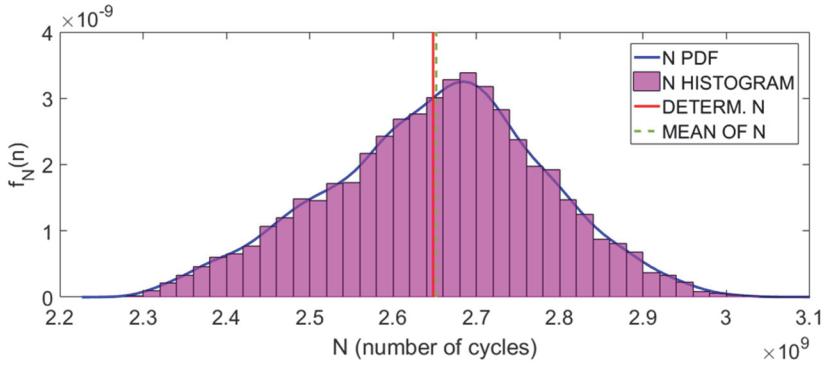

Figure 7: Histogram and PDF of SRQ $\boldsymbol{N}$ of the structural system with their corresponding indications: deterministic and mean.

Tabs. 4 and 5 present some statistical parameters referred to UIQs and SRQs treated herein. The values obtained from simulations performed are indicated as estimated in the pertinent columns. The relative errors are calculated between the deterministic and the simulated ones. The magnitudes of the relative errors obtained correspond to a good agreement of the simulations compared to the information initially provided, which is partially explained by the use of LHS as the method of uncertainty propagation. These tables also present the coefficient of variation (COV), in which UIQ a_0 could be observed as having the highest COV. Followed by a_0, in descending order, t, D, and m close this list of UIQs, i.e. the largest standard dispersion of the UIQs comes from a_0, and the smallest from m (the most efficient UIQ in recovering the previously given information). In addition, the relative errors shown in Tab. 5 address small magnitudes, highlighting that in what refers to lower and upper bounds, a_0 presents the largest values of relative error. In what concerns mean, t is the largest. In this case, the UIQ with the highest COV (a_0) also has the lowest efficiency to retrieve the previously given information. Therefore, it is important to note that the COV of a simulated UIQ is not always related to its efficiency in recovering the information given.

Parameter	*Estimated range*	*Estimated mean*	*Estimated standard deviation*
m	[2.9925; 3.0149]	3.0001	0.0058
a_0 (mm)	[2.4001; 2.6997]	2.5004	0.0777
$t(mm)$	[12.3001; 12.8999]	12.5022	0.1557
$D(mm)$	[272.3176; 274.3639]	273.0120	0.5332
$N(cycles)$	[2.2760; 3.0470] x 10^9	2.6490 x 10^9	0.1460 x 10^9

Table 4: Estimated range, mean, and standard deviation of the five main parameters.

Parameter	*RE of LB (%)*	*RE of UB (%)*	*RE of mean (%)*	*COV*
m	0.0001	0.0001	0.0031	0.0019
a_0 (mm)	0.0012	0.0127	0.0163	0.0311
$t(mm)$	0.0001	0.0010	0.0172	0.0125
$D(mm)$	0.0002	0.0004	0.0044	0.0020
$N(cycles)$	Not applicable	Not applicable	0.1360	0.0396

Table 5: Relative errors (RE) related to lower bound (LB), upper bound (UB), and mean, besides the coefficient of variation (COV) of the main parameters.

In what refers to the convergence of the means of the UIQs related to their deterministic values, a certain degree of stabilization of the means is achieved and the adoption of a criteria of 1×10^{-4} % is verified only at $N_r = 3957$, $N_r = 9787$, $N_r = 3662$, and $N_r = 3888$ realizations for UIQs m, a_0, t, and D, respectively. In the context of these simulations, the generated information leads to the conclusion that a_0 is the most restrictive parameter aiming at reducing the computational effort involved. In view of this, the number of realizations was selected to be 10000.

In addition to the bi-level sensitivity analysis (SA) performed, graphical SAs are presented in Figs. 8 and 9. These scatter plots represent a mapping of how the UIQs influence the behavior of the main SRQ N, which may help in decision making processes related to mechanical design and enable studies to reduce the dispersion based on the obtained information.

These plots also address the degree of dependence of N related to the involved UIQs, which can be represented herein by the correlation coefficient. Tab. 6 presents the correlation coefficients corresponding to the influence of the UIQs m, a_0, t, and D on the levels corresponding to their interaction with the SRQs S_r, K_r, da/dN, and N. From this table, when m goes from the first to the second level, the correlation is incremented significantly by 323.5%. However, the

correlation yet remains at a low level. In what refers to a_0, there is not a considerable increment from the first to the second level, but from the second to the third level, the correlation not only reduces to 18.6% of its contribution in the second level, but also becomes negative. The correlation coefficients that describe the behavior of t related to the first, second, and third levels maintain their tendency to low contribution to the SRQs involved in these levels. The fourth is 300.2% higher than the third, becoming more representative in the last level. Finally, D is an example of UIQ that starts with a low influence over the SRQ of the first level and finishes the calculation with a low contribution too. In a general manner, at fourth level, there is a weak correlation between the UIQs introduced in the first level.

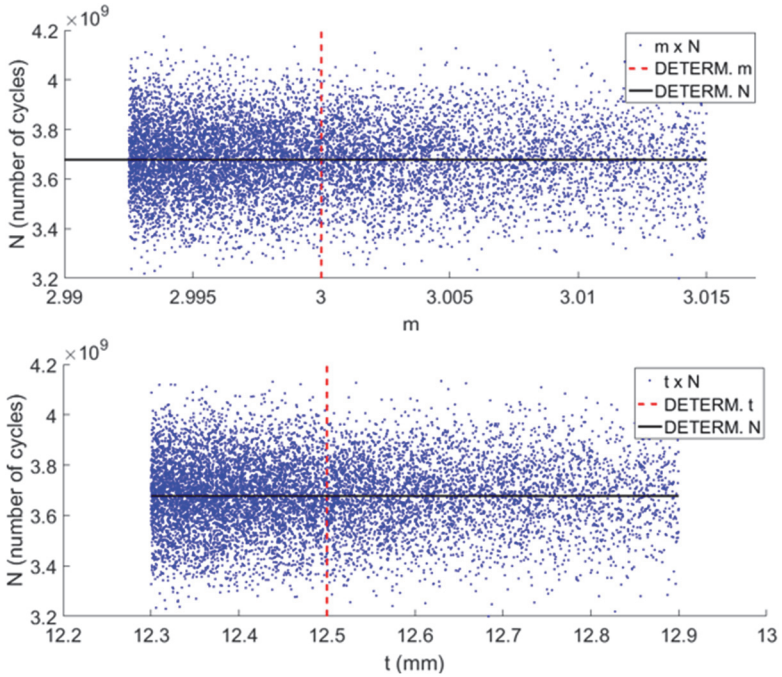

Figure 8: Scatter plots (graphical sensitivity analyses) of the UIQs m and t related to the SRQ N (element 2 as sample).

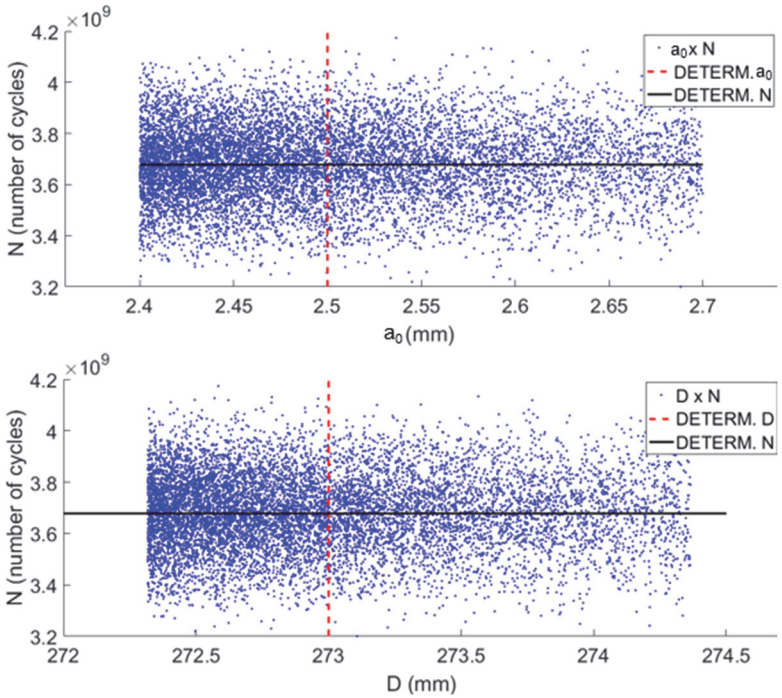

Figure 9: Scatter plots (graphical sensitivity analyses) of the UIQs a_0 and D related to the SRQ N (element 2 as sample).

Parameter	S_r	K_r	da/dN	N
m	Not applicable	Not applicable	-0.0053 (level 1)	-0.0223 (level 2)
a_0 (mm)	Not applicable	0.7271 (level 1)	0.7314 (level 2)	-0.1362 (level 3)
$t(mm)$	-0.0114 (level 1)	0.0211 (level 2)	0.0196 (level 3)	0.0785 (level 4)
$D(mm)$	0.0051 (level 1)	0.0137 (level 2)	0.0129 (level 3)	0.0054 (level 4)

Table 6: Correlation coefficients between UIQs and SRQs (parameters) in different levels.

Based on the information given by Tabs. 5 and 6, it can be observed that the highest standard dispersion (COV) and the highest correlation coefficients concomitantly come from UIQ a_0, which is also the least efficient in recovering the information of the expected value, lower and upper bounds. According to these same criteria, UIQ t is in the second position because it has the second highest COV and correlation coefficient concomitantly. Comparing m with D, the simulations retrieve the information with more accuracy in the former, with a lower COV, but higher correlation coefficient in the fourth level with the SRQ N.

As the second stage of the SAs performed in this paper, the first-order indices were calculated related to the SRQ N in order to reproduce the main effect contribution of each UIQ (m, a_0, t, and D) to the variance of the referred SRQ. This calculation yields the following rank of first-order sensitivity indices, in descending order: (a) $S_m = 0.9754$; (b) $S_D = 0.9722$; (c) $S_t = 0.6033$; and (d) $S_{a_0} = 0.4014$. In other words, the most impacting UIQ in the SRQ variance is m similar to the contribution of D. On the other hand, UIQ a_0 is the least significant to the variance of the SRQ N.

In what refers to design boundaries, Fig. 10 illustrates the behavior of SRQ da/dN with respect to UIQ K_r, which is a relation in the third level of calculation. Deterministic (blue points), minimum (red points), and maximum (yellow points) are shown for the last structural member that fails by fatigue (element 2), according to the corresponding labels. This cloud of points gives the mapping of the crack growth throughout the cycles related to the stress intensity factor range in order to provide the designer the information related to crack growth behavior. The fatigue crack growth boundaries (FCGBs) encompass the points that are within the contour composed of the most extreme points, thus forming a design envelope. This envelope may help in the prediction of the crack growth rate at a required confidence level, besides allowing the designer to adopt, for example, the worst-case crack growth scenario, in a conservative design. Therefore, under the given information, conditions, and assumptions, these FCGBs provide the most unbiased crack growth mapping.

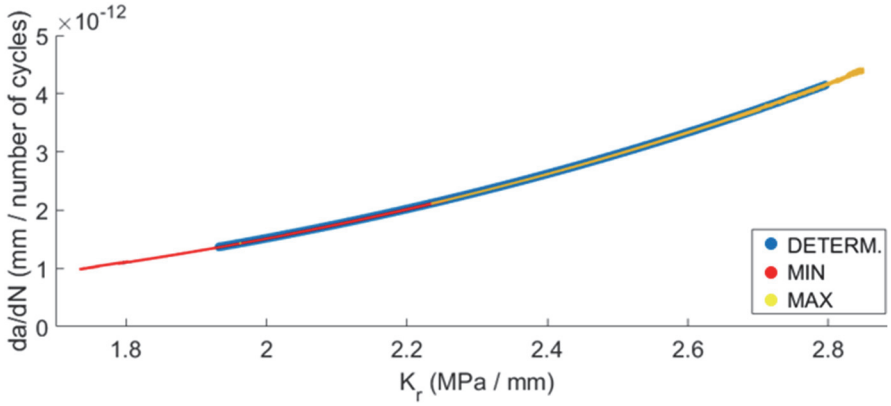

Figure 10: FCGBs produced by the family of curves da/dN *versus* K_r (element 2 as sample).

Fig. 11 also brings the concept of design boundaries, but now they are the fatigue crack semi-width boundaries (FCSBs), which delimit the allowable design region that relates the crack semi-width to the current number of stress cycles. Minimum (cloud of red points) is represented by the highest initial crack semi-width and the lowest fatigue life, whereas maximum (set of yellow points) presents the lowest initial crack semi-width and the highest fatigue life. The deterministic case is the set of blue points. The fatigue life corresponding to the minimum red cloud of points is $N_{min} = 2.2760 \times 10^9$ cycles, the one

corresponding to the deterministic curve is $N_{determ} = 2.4690 \times 10^9$ cycles, whereas the maximum is $N_{max} = 3.0470 \times 10^9$ cycles. These values of fatigue life correspond to the respective values of initial crack semi-width: $a_{0_{max}} = 2.6997\,mm$, $\tilde{a}_0 = 2.5004\,mm$, and $a_{0_{min}} = 2.4001\,mm$, as can be checked in Tab. 4. All the realizations that obey the imposed restrictions are within this region, each reaching a final crack semi-width of almost $a_f = 7.5000\,mm$ (corresponding to the most restrictive stopping criterion for this limit state). Therefore, according to the degree of risk the designer may take, the design can be more costly-effective.

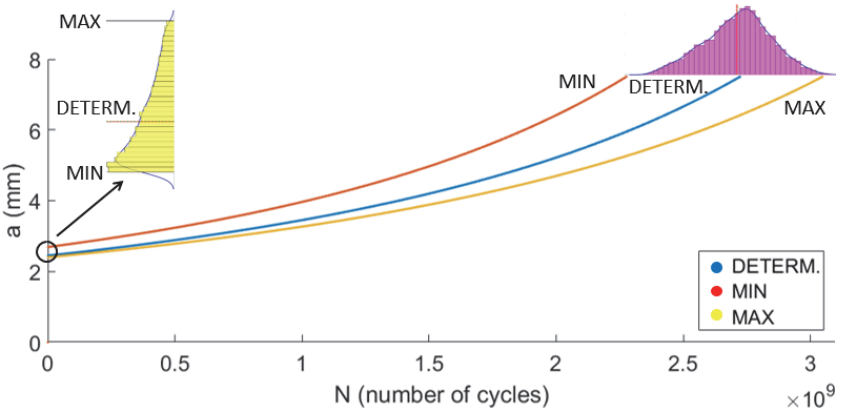

Figure 11: FCSBs produced by the family of curves $\boldsymbol{a}$ *versus* $\boldsymbol{N}$ (element 2 as sample).

The results obtained via this multi-level UQFW provide an allowable design envelope in order to predict the crack growth and semi-width at a determined confidence level. The deterministic case is shown as just one of the possibilities of occurrence because it is within the allowable region. Depending on the objectives set for a specific design, there will be a corresponding mechanical resistance offered. It is also important to note that in the case of more information available, the mathematical model has to be updated in order to fulfill the new requirements.

Therefore, FCGBs and FCSBs allow the designer to predict the worst-case fatigue scenario, besides being able to know the design range at a certain confidence level. Furthermore, the boundaries built up in this work provide the most unbiased fatigue crack growth and semi-width mappings under the conditions, assumptions, and simplifications made.

Conclusions

In this paper, a multi-level uncertain fatigue analysis was conducted using the strategy of an uncertainty quantification framework (UQFW), which was implemented in a tubular plane truss problem. The solution involves the induced-sequential fatigue failure of each structural member until the structure loses its functionality, simultaneously observing the criteria of material fracture toughness and maximum allowable crack semi-width. The uncertain input quantities (UIQs) considered herein were the geometrical parameters, material properties, and live loads. The main system response quantity (SRQ) obtained was the fatigue life, in the fourth level of calculation. This multi-level calculation of each structural member applied the finite element method (FEM) to find the stresses involved and the maximum entropy principle (MEP) to maximize the uncertainty related to the incomplete information provided. The SRQs of previous levels of calculation may enter as UIQs in the subsequent levels. The set of these levels corresponds to a round of calculation (each member failure). From this perspective, the main conclusions are as follows: 1. The multi-level uncertain fatigue analysis presented herein is able to produce the most unbiased range of possible solutions, thus maximizing the uncertainty, observing the limited available information. 2. The bi-level sensitivity analysis produced a rank of the most influencing fatigue design factors (UIQs), and addressed that the slope of the curve crack growth rate × stress intensity factor range (UIQ $\boldsymbol{m}$) influenced fatigue life the most. 3. The fatigue crack growth and fatigue crack semi-width boundaries (FCGBs and FCSBs) were established for the structure, simulating among others, the worst-, deterministic-, and best-case conditions. This mapping may be used as guidance to the designer to support decisions about crack growth rate and crack semi-width in existing cracks of the type treated herein, allowing the estimation of fatigue life of trusses.

Broadly, there is an increasing demand to develop the knowledge framework in fatigue predicting context. Fatigue life, dimensions of the components, crack growth rate, allowable crack semi-width, and the physical phenomenon itself are

only a few parts of this complex subject. In this direction, uncertainty quantification methods come to the aid of fatigue modeling, in order to yield a relatively safe design associated with the knowledge to perform increasingly reliable system assessments.

ACKNOWLEDGEMENTS

The author is very grateful to CEREARERM for the support under project number 01262113.

REFERENCES

[1] Campbell, F.C. (2012). Fatigue and Fracture: Understanding the Basics. Materials Park, ASM International.
[2] Mendoza, J., Nielsen, J.S., Sorensen, J.D. and Kohler, J. (2022). Structural Reliability Analysis of Offshore Jackets for System-level Fatigue Design. Structural Safety, 97, pp. 102220. DOI: 10.1016/j.strusafe.2022.102220.
[3] Qian, H.-M., Wei, J. and Huang, H.-Z. (2023). Structural Fatigue Reliability Analysis Based on Active Learning Kriging Model. International Journal of Fatigue, 172, pp. 107639. DOI: 10.1016/j.ijfatigue.2023.107639.
[4] Zhang, Z., Zhao, C., Zhao, Z., Wang, F. and Zhao, B. (2023). Structural Fatigue Reliability Evaluation Based on Probability Analysis of the Number of Zero-crossings Stochastic Response Process. Engineering Failure Analysis, 143, pp. 106923. DOI: 10.1016/j.engfailanal.2022.106923.
[5] Fan, J., Liao, H., Wang, H., Hu, J., Chen, Z., Lu, J. and Li, B. (2018). Local Maximum-entropy Based Surrogate Model and its Application to Structural Reliability Analysis. Structural and Multidisciplinary Optimization, 57, pp. 373-392. DOI: 10.1007/s00158-017-1760-y.
[6] Jing, G., Lyu, Z., Liu, Y., Xiao, S., Zhou, H. and Li, S. (2022). Reliability Study for Diesel Engine Cylinder Head through Fatigue Failure Analysis and Structural Optimization. Engineering Failure Analysis, 142, pp. 106768. DOI: 10.1016/j.engfailanal.2022.106768.
[7] Staroverov, O., Mugatarov, A., Yankin, A. and Wildermann, V. (2022). Description of Fatigue Sensitivity Curves and Transition to Critical States of Polymer Composites by Cumulative Distribution Functions. Frattura ed Integrità Strutturale, 17(63), pp. 91-99. DOI: 10.3221/IGF-ESIS.63.09.
[8] Kim, H.-S., Kim, B.W., Lee, K. and Sung, H.G. (2022). Application of Average Sea-state Method for Fast Estimation of Fatigue Damage of Offshore Structure in Waves with Various Distribution Types of Occurrence Probability. Ocean engineering, 246, pp. 110601. DOI: 10.1016/j.oceaneng.2022.110601.
[9] Yang, X., Fan, W. and Li, Z. (2022). Stochastic Analysis of Fatigue Damage of Transmission Tower-line System using Kriging and Bayesian Updated Probability Density Evolution Methods. International Journal of Structural Stability and Dynamics, 22 (3n04). DOI: 10.1142/S0219455422400090.
[10] Heng, J., Zheng, K., Kaewunruen, S., Zhu, J. and Baniotopoulos C. (2019). Dynamic Bayesian Network-based System-level Evaluation on Fatigue Reliability of Orthotropic Steel Decks. Engineering Failure Analysis, 105, pp. 1212-1228. DOI: 10.1016/j.engfailanal.2019.06.092.
[11] Li, Y., Zhi, P., Zhang, Y., Chen, B. and Wang, Y. (2020). Fatigue Reliability Analysis of Motor Hanger for High-Speed Train Based on Bayesian Updating and Subset Simulation. Advances in Materials Science and Engineering 2020, pp. 1-10. DOI: 10.1155/2020/3012471.
[12] Gray, A., Wimbush, A., De Angelis, M., Hristov, P.O., Calleja, D., Miralles-Dolz, E. and Rocchetta, R. (2022). From Inference to Design: a Comprehensive Framework for Uncertainty Quantification in Engineering with Limited Information. Mechanical Systems and Signal Processing, 165, pp. 108210. DOI: 10.1016/j.ymssp.2021.108210.
[13] Iskandar, R. (2021). Probability Bound Analysis: a Novel Approach for Quantifying Parameter Uncertainty in Decision-analytic Modeling and Cost-effectiveness Analysis. Statistic in Medicine, 40(29), pp. 6501-6522. DOI: 10.1002/sim.9195.
[14] Nonato, R.B.P. (2020). Bi-level Hybrid Uncertainty Quantification in Fatigue Analysis: S-N Curve Approach, Frattura ed Integrità Strutturale. 54, pp. 88-103. DOI: 10.3221/IGF-ESIS.54.06.
[15] Shannon, C.E. (1948). A Mathematical Theory of Communication, Bell System Technical Journal, 27(3), pp. 379-423.
[16] Jaynes, E. (1982). On the Rationale of Maximum-entropy Methods. Proceedings of the IEEE, 70(9), pp. 939-952.
[17] Ash, R.B. (1965). Information Theory. Urbana, Ash.

[18] Deely, J.J., Tierney M.S. and Zimmer W.J. (1970). On the Usefulness of the Maximum Entropy Principle in the Bayesian Estimation of Reliability. IEEE Transactions on Reliability, R-19(3), pp. 110-115.
[19] Picone, J. (1993). Signal Modeling Techniques in Speech Recognition. Proceedings of the IEEE, 81(9), pp. 1215-1247.
[20] Baggenstoss, P.M. (2014). Optimal Detection and Classification of Diverse Short-duration Signals. IEEE International Conference on Cloud Engineering, Boston, USA, 11-14 March. DOI: 10.1109/IC2E.2014.96.
[21] Ranganathan, R. (2006). Structural Reliability Analysis and Design. Mumbai, Jaico publishing house.
[22] Hertzberg, R.W. (1996). Deformation and Fracture Mechanics of Engineering Materials. New York, John Wiley and Sons.
[23] Park, J., Park, Y.C., Kim and H.K. (2018). A Methodology for Fatigue Reliability Assessment Considering Stress Range Distribution Truncation. International Journal of Steel Structures, 18, pp. 1242-1251. DOI: 10.1007/s13296-018-0104-0.
[24] Ghanem, R., Higdon, D. and Owhadi, H. (2017). Handbook of Uncertainty Quantification. Cham, Springer International publishing. DOI: 10.1007/978-3-319-12385-1.
[25] Papadopoulos, C., Hayes, B.K. and Newell, B.R. (2009). Non-Categorical Approaches to Property Induction with Uncertain Categories. Proceedings of the 31st Annual Conference of the Cognitive Science Society.
[26] Lloyd, S. and Ries, R. (2007). Characterizing, Propagating, and Analyzing Uncertainty in Life-Cycle Assessment: A Survey of Quantitative Approaches. Journal of Industrial Ecology, 11, pp. 161-179. DOI: 10.1162/jiec.2007.1136.
[27] Groen, E., Heijungs, R., Bokkers, E. and de Boer, I. (2014). Methods for Uncertainty Propagation in Life Cycle Assessment. Environmental Modelling and Software, 62, pp. 316-325. DOI: 10.1016/j.envsoft.2014.10.006.
[28] Ahmed, A. and Soubra, A.H. (2012). Extension of Subset Simulation Approach for Uncertainty Propagation and Global Sensitivity Analysis. Georisk: Assessment and Management of Risk for Engineered Systems and Geohazards, 6(3), pp. 162-176. DOI: 10.1080/17499518.2012.656296.
[29] Sheen, D.A. and Wang, H. (2011). The method of Uncertainty Quantification and Minimization using Polynomial Chaos expansions. Combustion and Flame, 158(12), pp. 2358-2374. DOI: 10.1016/j.combustflame.2011.05.010.
[30] Sundararajan, C.R. (1994). Probabilistic Structural Mechanics Handbook, Theory and Industrial Applications. New York, Springer Science.
[31] Oberkampf, R. and Roy, C.J. (2010). Verification and Validation in Scientific Computing. Cambridge, Cambridge university press. DOI: 10.1017/CBO9780511760396.
[32] Saltelli, A., Tarantola, S., Campolongo, F. and Ratto, M. (2004). Sensitivity Analysis in Practice: A Guide to Assessing Scientific Models. Chichester, John Wiley and Sons.
[33] Saltelli, A., Ratto, M., Andres, T., Campolongo, F., Cariboni, J., Gatelli, D., Saisana, M. and Tarantola, S. (2008). Global Sensitivity Analysis: The Primer. Chichester, John Wiley and Sons.
[34] Lu, H., Zhang, M.Y., Zhang, X. and Huang, X. (2011). Fatigue Reliability Sensitivity Analysis of Complex Mechanical Components under Random Excitation. Mathematical Problems in Engineering, 2011, pp. 1-17. DOI: 10.1155/2011/586316
[35] Qamar, S. (2014). Fracture Life Prediction and Sensitivity Analysis for Hollow Extrusion Dies. Fatigue and Fracture of Engineering Materials and Structures, 38, pp. 434-444. DOI: 10.1111/ffe.12244.
[36] Leander, J. and Al-Emrani, M. (2016). Reliability-based Fatigue Assessment of Steel Bridges Using LEFM – A sensitivity analysis. International Journal of Fatigue, 93, pp. 82-91. DOI: 10.1016/j.ijfatigue.2016.08.011.
[37] Amaro, R., Rustagi, N., Drexler, E. and Slifka, A. (2015). Sensitivity Analysis of Fatigue Crack Growth Model for API Steels in Gaseous Hydrogen. Journal of research of the National Institute of Standards and Technology, 119, pp. 6-14. DOI: 10.6028/jres.119.002.
[38] Sparkman, D., Millwater, H. and Ghosh, S. (2013). Probabilistic Sensitivity Analysis of Dwell-fatigue Crack Initiation Life for a two-grain Microstructural Model. Fatigue and Fracture of Engineering Materials and Structures, 36, pp. 994-1008. DOI: 10.1111/ffe.12052.
[39] Wang, Z., Huang, X. and Zhang, D.H. (2020). Low Cycle Fatigue Damage Model and Sensitivity Analysis of Fatigue Crack Initiation by Finite Element Approach. Frattura ed Integrità Strutturale, 14, pp. 81-91. DOI: 0.3221/IGF-ESIS.53.07.
[40] Zhu, S.P., Liu, Q., Yu, Z.Y. and Liu, Y. (2017). Fatigue Reliability Analysis of a Turbine Disc under Multi-source Uncertainties. 2nd International Conference on Structural Integrity, Funchal, Portugal. DOI: 10.1016/j.prostr.2017.07.137.
[41] Morris, M. (1991). Factorial Sampling Plans for Preliminary Computational Experiments. Quality Engineering, 37, pp. 307-310.

[42] Shamilov, A., Kantar, Y.M. and Ilhan, U. (2008). Use of MinMaxEnt Distributions Defined on Basis of MaxEnt Method in Wind Power Study. Energy Conversion and Management, 49, pp. 660-677. DOI: 10.1016/j.enconman.2007.07.045.
[43] Zu, T., Kang, R., Wen, M. and Zhang, Q. (2018). Belief Reliability Distribution Based on Maximum Entropy Principle. IEEE Access, 6, pp. 1577-1582. DOI: 10.1109/ACCESS.2017.2779475.
[44] Kang, H.Y. and Kwak, B.M. (2008). Application of Maximum Entropy Principle for Reliability-based Design Optimization. Struct, Multidisc. Optim., 38, pp. 331-346. DOI: 10.1007/s00158-008-0299-3.
[45] Zhang, Y. (2018). Principle of Maximum Entropy for Reliability Analysis in the Design of Machine Components. Frontiers of Mechanical Engineering, 14, pp. 1-12. DOI: 0.1007/s11465-018-0512-z.
[46] Guo, J., Zhao, J. and Zeng, S. (2018). Structural Reliability Analysis Based on Analytical Maximum Entropy Method Using Polynomial Chaos Expansion. Struct. Multidisc. Optim., 38, pp. 1187-1203. DOI: 10.1007/s00158-018-1961-z.
[47] Jiwei, Q., Jianguo, Z. and Yupeng, M. (2018). Reliability Analysis Based on the Principle of Maximum Entropy and Dempster–Shafer Evidence Theory. Journal of Mechanical Science and Technology, 32, pp. 605-613. DOI: 10.1007/s12206-018-0107-3.
[48] Jaynes, E. (1957). Information Theory and Statistical Mechanics. Physical Review, 106, pp. 620-630.
[49] DeMarte, R.A. (2009). Analysis of Fatigue Crack Propagation in Welded Steels. Master's thesis. Marquette, Milwaukee.
[50] Lampman, S. (1996). ASM Handbook: Fatigue and Fracture. Detroit, ASM International.
[51] Frank, K.H., Barsom, J.M. and Hamburger, R.O. (2000). State of the Art Report on Base Metals and Fracture. Tech. rep., Federal Emergency Management Agency.